

# The Source of Hydrogen in Earth's Building Blocks

Thomas J. Barrett<sup>1</sup>, James F.J. Bryson<sup>1</sup>, Kalotina Geraki<sup>2</sup>

1. Department of Earth Sciences, University of Oxford, Oxford, OX1 3AN, UK.
2. Diamond Light Source, Harwell Science and Innovation Campus, Didcot, OX11 0DE, UK.

Thomas Barrett

Email: [thomas.barrett@st-annes.ox.ac.uk](mailto:thomas.barrett@st-annes.ox.ac.uk)

## Abstract

Despite being pivotal to the habitability of our planet, the process by which Earth gained its present-day hydrogen budget is unclear. Due to their isotopic similarity to terrestrial rocks across a range of elements, enstatite chondrites (ECs) are thought to be the meteorites that best represent Earth's building blocks. Because of ECs' nominally anhydrous mineralogy, these building blocks have long been presumed to have supplied negligible hydrogen to the proto-Earth. Instead, hydrogen has been proposed to have been delivered to our planet after its main stage of formation by impacts from hydrated asteroids. In this case, our planet's habitability would have its origins in a stochastic process. However, ECs have recently been found to unexpectedly contain enough hydrogen to readily explain Earth's present-day water budget. Although this result would transform the processes we believe are required for rocky planets to be suitable to life, the mineralogical source of ~80% of hydrogen in these meteorites was previously unknown. As such, the reason ECs are seemingly rich in hydrogen was unclear. Here, we apply sulfur X-ray absorption near edge structure (S-XANES) spectroscopy to ECs, finding that most (~70%) of their hydrogen is bonded to sulfur. Moreover, the concentration of the S-H bond is intimately linked to the abundance of micrometre-scale pyrrhotite ( $\text{Fe}_{1-x}\text{S}$ ,  $0 < x < 0.125$ ), suggesting most hydrogen in these meteorites is carried in this phase. These findings elucidate the presence of hydrogen in Earth's building blocks, providing the key evidence that unlocks a systematic, rather than stochastic, origin of Earth's hydrogen.

## Significance statement

Although water plays a crucial role in Earth's habitability, the reasons behind its presence on our planet are unclear. Historically, Earth is thought to have formed through the accumulation of 'dry' material, with water and other volatile species being delivered millions of years later. Contrarily, recent studies have found that meteorites closely resembling Earth unexpectedly contain high hydrogen concentrations. However, the reason behind this enrichment was unclear. To explore their source of hydrogen, we applied X-ray absorption spectroscopy to Earth-like meteorites. We found significant concentrations of hydrogen in micron-scale grains of iron sulfide. This argues that Earth, and potentially other terrestrial planets, contained significant quantities of the hydrogen from their inception, aiding their suitability for life.

## Introduction

Although water is central to planetary habitability as we know it, the mechanism by which Earth gained its substantial present-day water budget is unclear. Enstatite chondrites (ECs) closely resemble terrestrial rocks across a range of isotopic compositions<sup>1</sup>. Hence, ECs (or material similar to these meteorites) have been suggested as the predominant building blocks of the proto-Earth<sup>2</sup>, as well as other terrestrial planets including Mars<sup>3</sup>. ECs formed in the hot inner solar system, so consist entirely of nominally anhydrous minerals<sup>4</sup>. As such, Earth's building blocks have long been presumed to have been 'dry', so provided negligible hydrogen to the proto-Earth<sup>5,6</sup>.

Several processes have been suggested to have then provided water to our planet later in its history. These include a late veneer of hydrated cometary material<sup>7</sup>, and delivery via bombardment from outer-solar-system derived carbonaceous chondrite material<sup>8</sup>. These models imply that our planet's water budget – and by extension, its suitability for life – is the result of the stochastic scattering of outer solar system material into the terrestrial planet forming region<sup>6</sup>. As such, habitability would not be a natural consequence of Earth's formation from enstatite chondrite-like material.

Contrary to early observations, recent measurements of the bulk compositions of ECs reveal they unexpectedly contain high concentrations of hydrogen<sup>9,10</sup>. Indeed, these meteorites seemingly carry enough hydrogen to account for up to ~14 times the mass of Earth's oceans. Moreover, isotopic measurements argue that Earth accreted ~70% of its volatile inventory, including hydrogen and nitrogen, from inner Solar System material<sup>9,11,12,13</sup>. Combined, these findings indicate that Earth, and other terrestrial planets, may have in fact formed with high initial inventories of hydrogen and other volatiles.

Despite this high bulk concentration, it is not clear how or why ECs are rich in hydrogen. Previous studies<sup>9</sup> were able to account for only ~20% of the bulk EC hydrogen content in chondrule mesostasis and insoluble organic matter (IOM)<sup>14</sup>. Additionally, later work<sup>15</sup> demonstrated a link between hydrogen and sulfur concentrations in chondrule mesostasis, but did not identify the ultimate mineralogical source of hydrogen. While the source of ~80% of the bulk hydrogen in ECs remains unknown, our ability to adopt these high hydrogen concentrations reliably and understand how Earth gained its water budget is limited. Here, we map ECs using micrometre-scale X-ray absorption near edge structure spectroscopy at the sulfur K edge (S-XANES) to explore the source and carrier of hydrogen in these meteorites.

## Results

We measured a map of S-XANES spectra with 5  $\mu\text{m}$  resolution in a region of clastic matrix in the EH3 chondrite LAR 12252. We also collected 15 spot spectra from chondrule mesostasis as well as several spot spectra from two cracks. These spectra were measured at beamline I18 at the Diamond Light Source. The region of matrix we investigated included fragments of chondrule mesostasis and enstatite, grains of metal and sulfides, and fine matrix (composed of an assortment of materials, all <5  $\mu\text{m}$  large). S-XANES spectra of fine matrix and mesostasis typically contain four clear peaks (Figure 1a), providing evidence of sulphur in different compounds and oxidation states. By comparing peak energy and shape to reference spectra<sup>16–18</sup>, we can identify the species responsible for each peak (Table. S1).

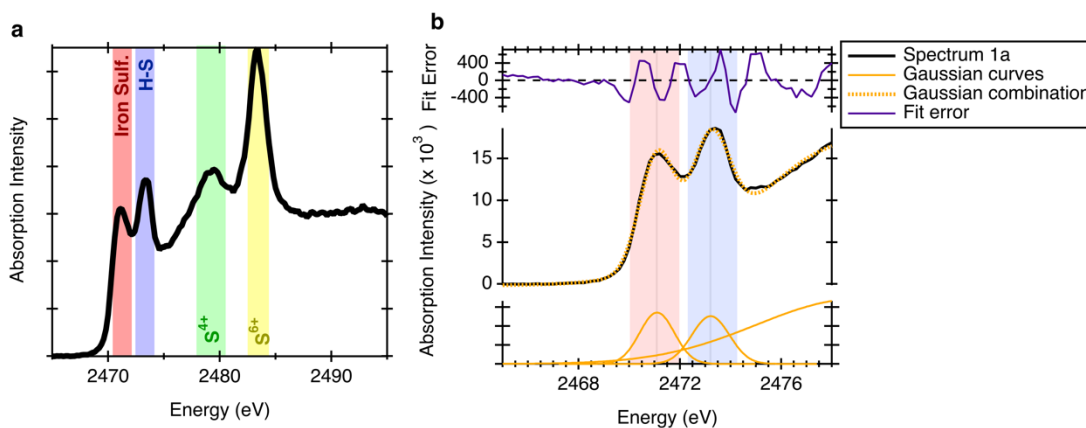


**Figure 1a** S-XANES spectrum from a point in fine matrix in LAR 12252. Positions of peaks ascribed to species from reference spectra<sup>16–18</sup> are highlighted by vertical coloured bars. **1b** Peak fitting method used to extract the amplitudes of the iron sulfide and H-S peaks. We achieved this by creating a total fit (dashed orange in middle panel) from three

Gaussian curves (orange, bottom panel) across the energy range 2468-2478 eV. This process yields small residual errors (purple, top panel). The highlighted peaks correspond to the same as in figure 1a.

The peak at lowest energy, highlighted in red in Figure 1, is widespread in fine matrix and mesostasis and is ascribed to submicron-scale iron sulfides (troilite and pyrrhotite)<sup>16,19–21</sup>. The energy of this peak varies from 2471.8eV to 2471.2eV, diagnostic of the composition of this mineral shifting from stoichiometric troilite to pyrrhotite ( $\text{Fe}_{1-x}\text{S}$ ,  $0 < x < 0.125$ )<sup>22</sup>. All energies in our spectra are slightly ( $\sim 1$  eV) higher than reported in most previous studies<sup>16,19–21</sup>. Such variations are common in XANES studies and are attributed to differences in calibration of the monochromator (table S1).

Throughout the fine matrix, we also find a distinctive peak at  $\sim 2473.2$  eV, highlighted in blue in figure 1. Based on previously reported spectra<sup>18,20,23</sup>, we ascribe this peak to sulfur bonded to hydrogen. The widespread nature of this peak in this material demonstrates that H-S is a common form of hydrogen in ECs, extending the findings from ref. 15 to a wider range of phases. Additionally, we detected the H-S peak in 15 spot spectra across 7 different chondrules within LAR 12252, supporting previous observations of H and the H-S bond in chondrule mesostasis<sup>15</sup>.

In addition to reduced sulphides, many spectra also contain peaks corresponding to the presence of  $\text{S}^{6+}$ , the most oxidised form of sulphur, highlighted yellow in figure 1. These peaks are at their highest amplitudes in spot spectra collected within cracks where clear terrestrial weathering has occurred (Fig. S3). They also exist at much lower amplitudes in matrix and mesostasis. Sulfates can be difficult to distinguish from each other using S-XANES because different cations do not cause significant shifts in peak energy<sup>16</sup>. Despite this, we identified  $\text{CaSO}_4$  and  $\text{FeSO}_4$  at some points in the meteorite, owing to minor peaks in the pre- and post-edge regions of the spectra<sup>16</sup>. The  $\text{S}^{6+}$  peak is absent within macroscopic ( $>10$   $\mu\text{m}$ ) grains of metal, enstatite, and sulfides.

Additionally, we observe a small amplitude peak centred on  $\sim 2478$ eV, shown in green in figure 1. The amplitude of this peak is affected by the presence of two species, a second wide absorption feature of troilite and pyrrhotite, and small amounts of  $\text{S}^{4+}$  likely formed through gradual photo-reduction of  $\text{S}^{6+}$  by the X-ray beam<sup>17,24</sup>. We minimised the impact of photoreduction mapping with short acquisition times.

Because peak amplitude correlates with species abundance<sup>16,19</sup>, we are able to constrain the concentrations of the different species in the matrix of LAR 12252 using XANES spectra. While the nature of complex geological samples like meteorites introduces specific challenges, we chose to estimate the concentration of H-S by comparing the amplitude of the peak at 2473.2 eV throughout our map to that of a phase with known H concentration, namely mesostasis. This chondrule glass has previously had its hydrogen concentration measured using background-corrected nano-secondary ion mass spectrometry<sup>9,15</sup> (see SI). We measured 15 spot S-XANES spectra of chondrule mesostasis in LAR 12252, and used these to determine an average H-S peak amplitude for this phase (Fig. S8). We found our clastic matrix region contains H-S peak amplitudes that vary from  $\sim 0.1$ -50 times average mesostasis (Figure 2b). The lowest relative amplitudes are found within the interiors of macroscale enstatite, metal, and sulfide grains. The highest amplitudes are in regions of fine matrix. Adopting an average concentration of H in chondrule mesostasis of 706 ppm<sup>9,15</sup> and excluding points with extensive terrestrial weathering (in the form of sizeable  $\text{S}^{6+}$  peaks; fig S5), we calculate that fine matrix in LAR 12252 contains an average of  $\sim 5880$  ppm H. For a clastic matrix abundance of 9.6 wt% of the bulk meteorite<sup>25,26</sup>, and a fine matrix abundance of 50 wt% of the clastic matrix<sup>27</sup>, the fine matrix accounts for  $\sim 4.8$  wt% of the bulk meteorite. This material therefore contributes an average of  $\sim 283$  ppm H to the bulk concentration in EH3 chondrites. As such, it accounts for  $\sim 60$  wt% of the total H budget<sup>9</sup>.

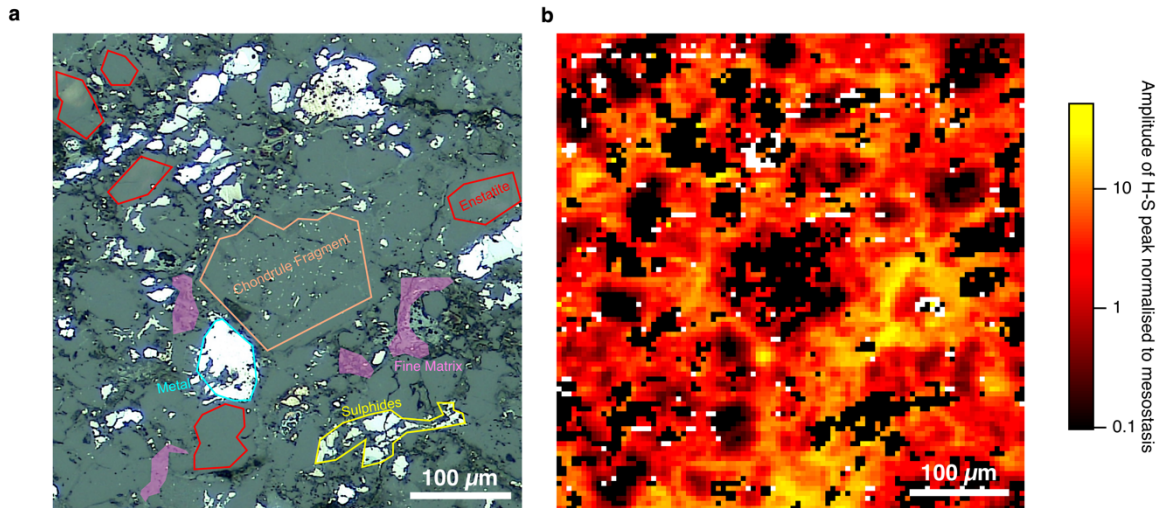


**Figure 2a** Optical image of the clastic matrix region in LAR 12252 that was studied using S-XANES. Notable phases include enstatite (example outlined in red), sulphides (example outlined in yellow), a small chondrule fragment (outlined in orange), and fine matrix (example highlighted in pink). **b** Corresponding map calculated from the S-XANES spectra of the region shown in **a**, showing the amplitude of the H-S peak at each point normalised to the average amplitude of point spectra measured from chondrule mesostasis. Black pixels correspond to points where the S-XANES spectra that did not contain a resolvable H-S peak. White pixels correspond to points where the S-XANES spectra could not be fitted due to their quality or noise in the spectra.

## Discussion

### Is EC H native or a product of terrestrial weathering?

The primary difficulty with measuring the hydrogen content of a meteorite is ensuring that the hydrogen is not a terrestrial weathering product. This is especially pertinent in enstatite chondrites, where rare sulphide phases such as oldhamite react readily with atmospheric moisture to produce hydrated sulfates<sup>28,29,30</sup>. While we avoided areas with extensive visible terrestrial weathering products, such as rust, much of the remaining meteorite could still have been modified by terrestrial weathering. As such, it has been suggested that previous measurements of bulk EC hydrogen concentrations were substantially influenced by the presence of terrestrial water/OH<sup>-</sup> contained in weathering products<sup>10,31</sup>.

Figure 1 shows a clear peak at 2483.4 eV, attributed to the presence of oxidised, S<sup>6+</sup>-bearing species. However, the pre-terrestrial minerals found in particularly pristine ECs (including niningerite, oldhamite, and Si-bearing metal) argue these meteorites formed under particularly reducing conditions<sup>4</sup>. As such, the presence of S<sup>6+</sup> bearing phases is most easily explained as a product of terrestrial weathering. This is reinforced by spot spectra measured from rust-bearing cracks in the meteorite, which contained the highest S<sup>6+</sup> peak amplitudes we measured (Fig. S3). Additionally, another crack contains pyrrhotite that has formed through the reaction of terrestrial water with native troilite in the meteorite (Fig. S4). Fortunately, the presence of this S<sup>6+</sup> peak allows us to monitor the extent of terrestrial alteration at each point measured, and identify the phases created by the weathering process. Crucially, these crack spectra contain either no resolvable H-S peak at 2473.2 eV (the crack containing terrestrial pyrrhotite, fig. S4), or one of very small amplitude relative to the S<sup>6+</sup> peak (fig. S3), demonstrating that H-S is not a weathering product. Therefore, H-S appears to be native to EH3 meteorites.

Nonetheless, in order to minimise any unidentified influence of terrestrial weathering, we chose to exclude spectra with an S<sup>6+</sup>:FeS peak amplitude ratio >0.5 in our analysis (see SI). Given the weathering induced reaction of FeS to H<sub>2</sub>SO<sub>4</sub> proposed to occur in chondrites<sup>29</sup>, adopting this ratio ensures we analysed only the least weathered spectra from within our mapped region.

## Abundance of H

Our analysis demonstrates that H-S exists in multiple phases in ECs and is in highest concentration in fine matrix. This phase accounts for ~60% of the bulk hydrogen value<sup>9</sup>, arguing it is the dominant source of H in Earth's building blocks, capable of explaining ~9 times Earth's entire estimated present-day ocean water budget<sup>9</sup>.

Previous studies have observed a relationship between S and H concentrations in mesostasis and have observed the S-H bond in this phase using Raman spectroscopy<sup>15</sup>. Together with our observation of the S-H bond in mesostasis and fine matrix from S-XANES, S-H appears to be the predominant carrier of hydrogen in EH3 chondrites, accounting for ~70% of their bulk budget (Fig. 3). Combining our concentration estimate from fine matrix with previously measured concentrations of hydrogen in IOM<sup>14</sup>, we can now ascribe a source and carrier of ~80% of the bulk hydrogen budget of EH3 chondrites (Figure 3).

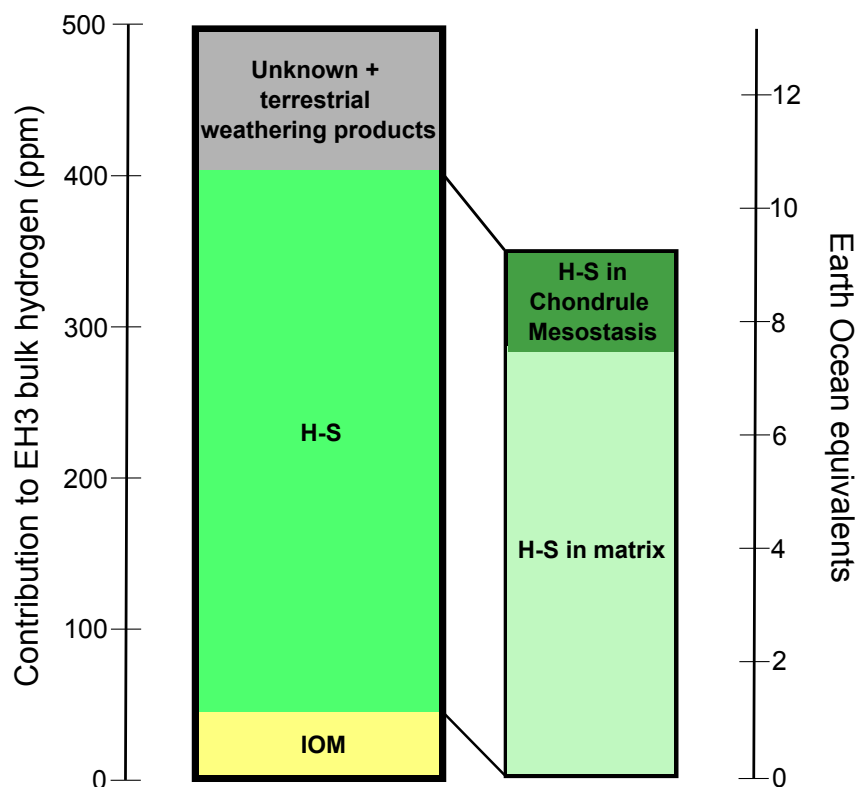


**Figure 3** Relative contributions of different phases to the bulk EH3 hydrogen concentration<sup>9</sup>. The concentration from IOM is taken from ref 14. The concentration in chondrule mesostasis is taken from refs 9,15. The concentration of H-S in matrix is from this study. We assume the unaccounted proportion of hydrogen is associated with unexplored phases and terrestrial weathering products. Right hand axis shows the relative contributions in terms of their Earth ocean equivalent, based on the accretion of Earth by 100% EC-like material, where the mass of 1 ocean is  $1.4 \times 10^{21}$  kg ref. 9.

## Source of H

Despite appearing to host most of the hydrogen in enstatite chondrites, the phase that carries the H-S bond we identified, and how it formed, were previously unknown. It is possible that a gaseous H-S-bearing species, such as  $H_2S$ , could have adsorbed onto grain surfaces from the solar nebula. However, this process is not expected to sequester large concentrations of H because it involves only very thin layers on the surfaces of grains.

Instead, we found that spectra with large H-S peak amplitudes also exhibited large Fe-S peak amplitudes. In fact, the ratio of these two peak amplitudes varies between only ~0 – 1 (Figure 4)

despite absolute amplitudes of these peaks varying by several orders of magnitude throughout our field of view (Fig. S2). This relationship suggests that the concentration of H-S is linked to the abundance of iron sulfides.

This variation in relative peak amplitudes can be used to further explore the origin of H in ECs. We found that spectra with a resolvable H-S peak (i.e., ratio of H-S peak amplitude to iron sulfide peak amplitude >0) tend to contain an iron sulfide peak at lower energies than those that do not contain a resolvable H-S peak (Figure 4a). The energy of the iron sulfide peak depends on the stoichiometry of this phase, with the peak shifting the lower energy as the mineral become more iron deficient (i.e., as the mineralogy evolves from troilite to pyrrhotite<sup>22</sup>). As such, this observation suggests that H is associated with pyrrhotite in ECs.

We can explore this in more detail by examining the relative peak amplitude of each individual spectrum. We find a clear trend between the energy position of each sulfide peak and the relative peak amplitude of the H-S peak (Figure 4b). This relationship further indicates that the abundance of the H-S bond in the sulfide increases gradually as the sulfide loses Fe. Together, these observations argues that pyrrhotite is the source of H, which appears to substitute for Fe.

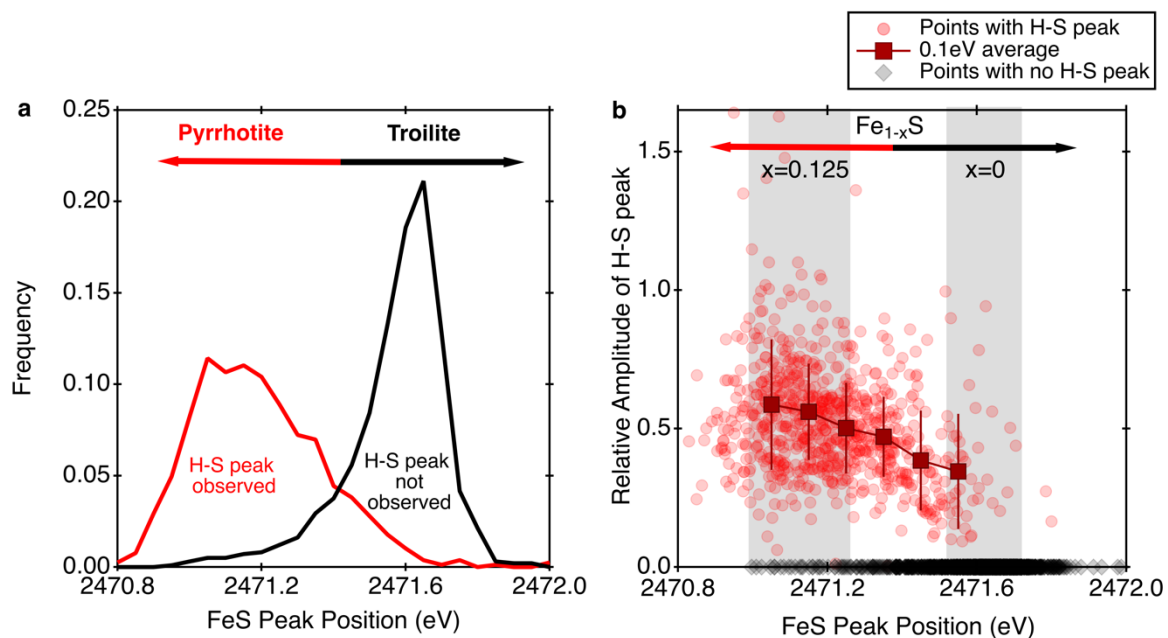


**Figure 2a** The distribution of the position of the FeS peak throughout the mapped area for spectra with (red) and without (black) resolvable H-S peaks. Spectra with energies of the iron sulfide peak that indicate pyrrhotite are more likely to carry the H-S peak, while spectra with iron sulfide peak energies consistent with troilite are less likely to display an H-S peak. **b** The amplitude of the H-S peak normalised to the amplitude of the corresponding FeS peak from each spectrum, plotted against the peak position of the FeS peak. Grey bars indicate the peak location of end member FeS (troilite) and pyrrhotite. The transition between these bars represents a change in  $x$  in the pyrrhotite chemical formula,  $\text{Fe}_{1-x}\text{S}$ ,  $0 < x < 0.125$ . Black diamonds on the horizontal axis represent spectra with no resolvable H-S peak. The dark red squares represent averages of the individual points in 0.1 eV-wide bands. The relative amplitude of the H-S peak increases as the abundance of pyrrhotite increases, further suggesting pyrrhotite is the carrier of H in enstatite chondrites.

The presence of pyrrhotite in ECs is perhaps unexpected given the reducing nebula environment in which these meteorites formed<sup>4,32</sup>. Previous measurements of the concentrations of iron sulfides in ECs made using electron probe micro analysis find near-stoichiometric compositions<sup>32,33</sup>. Our XANES spectra support this result, with the spectra from the centre of macroscopic sulfides ( $\geq 10 \mu\text{m}$ ) matching reference spectra of troilite. However, in the fine matrix and approaching the edges of some macroscopic sulfide grains, the energy of the Fe-S peak shifts to lower values. This shift argues that pyrrhotite exists as micron- to sub-micron-scale grains in fine matrix and micron- to

sub-micron-scale rims on larger troilite grains. Although nebular troilite is more common, nebular pyrrhotite has been observed previously as rims of pyrrhotite  $\sim 50$  nm wide coating larger grains of troilite in carbonaceous chondrites<sup>34</sup>, in the matrix of ECs as submicron grains<sup>25</sup>, and as  $<50$  nm grains in anhydrous IDPs<sup>35</sup>. These observations argue that when these sulphides are sub-micron in scale they exist as pyrrhotite. This pyrrhotite has been proposed to have formed through low temperature sulfidation of pre-existing troilite in a high  $f_{S_2}$  environment in the disk<sup>34-36</sup>, or alternatively through the sulfidation of Fe metal by  $H_2S$ <sup>37</sup>. Our results suggest this former processes occurred only on the outer part (perhaps  $<1 \mu m$ ) of troilite grains, which would cause an entire troilite grain to transform to pyrrhotite if it was below this critical size. Our findings suggest that  $H_2$  from the disk reacted into the pyrrhotite structure, perhaps into the Fe vacancy, during the low-temperature sulfidation of troilite. This process enabled high concentrations of hydrogen to be locked into this phase in enstatite chondrites. Matrix in these meteorites therefore has the ideal mineralogy (i.e., abundant sub-micron sulfides) and formation environment (i.e., in an  $S_2$ -rich and  $H_2$ -rich gas) to store appreciable hydrogen in the form H-S bonds in pyrrhotite.

The presence of sulfides in the spectra of points in the mesostasis mean it is plausible that H-S in mesostasis is also present within sub-micron sulfide grains in the mesostasis.

### Implications

In conventional models of the origin of volatile elements on Earth, water was the result of stochastic, late bombardment of carbonaceous material onto our planet<sup>8</sup>. This scenario is capable of explaining Earth's water budget, but means that water and habitable conditions on Earth are a result of a chance scenario. The combined D and  $^{15}N$  compositions of the oceans and atmosphere compared to the mantle<sup>9</sup> indicate that there is a contribution from this carbonaceous source, at least on the surface of our planet. However, this cannot explain the bulk of the hydrogen throughout our planet<sup>9</sup>, and instead likely only corresponds to a small proportion of the total H budget of Earth.

Our findings suggest that pristine enstatite chondrites contain enough hydrogen to explain the entire water budget of our planet, requiring that less water is needed to have been delivered to our planet. In this scenario, enstatite chondrites seemingly became enriched in hydrogen through sulfidation of troilite in an  $S_2$ -rich and  $H_2$ -rich nebular gas. As such, the water budget of Earth, is not the result of a chance bombardment. Instead, it can be a natural consequence of the formation of enstatite chondrite-like material in the hot, reducing and sulfidising environment of the inner solar system. Additionally, this means that other terrestrial planets that have been proposed to have formed from similar material – including Mars<sup>3</sup>, Mercury<sup>38</sup>, and perhaps Venus – may have had similar early volatile budgets to that of the proto-Earth. A key question that now exists is the hydrogen content of metamorphosed EHs (EH4-EH6), aubrites, and the proportion of each of these types of meteorites in the proto-Earth.

### Conclusions

To explore the source of hydrogen in Earth's building blocks, we analysed the EH3 chondrite LAR 12252 using micrometre-scale S-XANES spectroscopy. We find hydrogen throughout this meteorite bonded to sulfur, detected by a peak at 2473.2 eV. This form of hydrogen exists in chondrule mesostasis, as well as in areas of fine matrix at notably higher concentrations (up to a factor of  $\sim 50$  times richer in fine matrix relative to mesostasis). Spectra of areas of clear terrestrial weathering (i.e., cracks) demonstrate that hydrogen bonded to sulfur is not brought into this meteorite through this process. Including hydrogen previously identified in chondrule mesostasis, the carrier of the majority of hydrogen ( $\sim 70\%$ ) in enstatite chondrites can now be ascribed to H-S. The abundance of H-S is also intricately linked to the concentration of pyrrhotite. This sulfide exists in enstatite chondrites as sub-micron grains in the fine matrix as well as possibly narrow

rims surrounding macroscopic grains of troilite. Pyrrhotite is thought to form through the sulfidation of troilite at low temperature in the protoplanetary disk. We propose that during this process, H<sub>2</sub> from the disk bonded to S in the pyrrhotite, becoming trapped in its crystal structure, perhaps within the Fe vacancy. As a result, the reducing, sulfur-rich environment in which enstatite chondrites formed resulted in a pathway through which nebula hydrogen was sequestered into these meteorites. As such, hydrogen enrichment – and by extension, potentially habitable planetary chemistries – appear to be a natural consequence of formation from reduced material in the terrestrial planet forming region of the solar system.

## Materials and Methods

We explored the speciation and abundance of S in the EH3 chondrite LAR 12252, an Antarctic find, using micrometre-scale S-XANES at beamline I18 at Diamond Light Source. We chose to study LAR 12252 due to its low weathering grade of A (ref. 39), which minimises the likelihood of widespread or prevalent terrestrial H-bearing weathering products. We studied a thin section (LAR 12252) from the Antarctic Meteorite Collection.

We constructed 2D S-XANES maps of an area of clastic matrix material in this meteorite by sweeping a beam with a 5 μm spot size in 5 μm steps over an area 470 × 480 μm<sup>2</sup> large, resulting in a total of 9,024 spectra. The energy of the beam was increased from 2465-2495 eV in 0.2 eV intervals at each individual spot, with an acquisition time of 0.05 s for each energy value. The mapped area was selected to target clastic matrix, avoiding regions containing any large grains (≥100 μm) or obvious signs of terrestrial weathering, such as rust. We also measured 15 spot spectra at points within chondrule mesostasis, as well as in cracks containing terrestrial weathering products. Chondrule mesostasis spots were selected following optical microscopy, ensuring that they represented the range of chondrules present in the thin section while including regions of mesostasis suitable for XANES analysis.

To exclude points in the matrix region we mapped with more prevalent weathering, we only included points with S<sup>6+</sup>:FeS peak amplitude ratio <0.5 in our analysis. We selected this threshold to include only the least weathered points, while still maintaining a significant sample size for analysis (>750 spectra).

Peak fitting was conducted in IGOR Pro using a Gaussian multi-peak fitting method, discussed further in the SI. This method was selected over linear combination fitting due to the heterogeneities within the sample, absence of a complete reference database of spectra collected from meteorites, and the number of spectra collected. We chose to fit the spectra only between 2465-2478 eV (fig. 1b) because this energy range contains the iron sulfide peak, the H-S peak, and parts of the S-edge step function and peak due to S species at higher energies. We chose this approach because it allowed us to focus on the peaks of interest, making the fitting procedure more robust and straightforward. As seen in Figure 1, this method produced only small fitting errors. To determine the amplitude of the S<sup>6+</sup> peak, we simply fitted a single Gaussian curve in the energy range 2580-2590 eV. This approach means the recovered height of this peak is that above the background in this energy range. To quantify the enrichment/depletion of hydrogen in the form of H-S in matrix compared to mesostasis, we normalised the amplitude of the H-S peak recovered from each point in matrix to the average amplitude recovered from 15 spot spectra from chondrule mesostasis. To convert these ratios to an average H concentration, we calculated an average H enrichment factor from fine matrix and adopted an average value of H in chondrule mesostasis (measured using nano-SIMS) of 706 ppm(ref 9,15) (see SI).

Given that our spectra from mesostasis indicate that submicron sulfides exist in the glass, it is plausible that the hydrogen in mesostasis is also hosted in grains of pyrrhotite, as in the fine



matrix. In this case, the carrier phase of H in both mesostasis and matrix would be the same, and we therefore chose not to apply a correction for the phase that carries hydrogen when calculating the hydrogen concentrations from mesostasis values.

### Acknowledgements

The authors would like to thank Diamond Light Source for beamtimes (proposals SP31591-1 and SP35606), and staff of beamline I18 for assistance with data collection. The authors would also like to thank the Antarctic Search for Meteorites (ANSMET) program (which has been funded by NSF and NASA and curated by the Department of Mineral Sciences of the Smithsonian Institution and Astromaterials Curation Office at NASA Johnson Space Center) for use of their meteorite samples. JFJB acknowledges funding through UKRI grant number EP/Y014375/1. TJB acknowledges funding through STFC.

### References

1. Dauphas, N. The isotopic nature of the Earth's accreting material through time. *Nature* **541**, 521–524 (2017).
2. Javoy, M. *et al.* The chemical composition of the Earth: Enstatite chondrite models. *Earth and Planetary Science Letters* **293**, 259–268 (2010).
3. Brasser, R., Dauphas, N. & Mojzsis, S. J. Jupiter's Influence on the Building Blocks of Mars and Earth. *Geophysical Research Letters* **45**, 5908–5917 (2018).
4. Weisberg, M. K. & Kimura, M. The unequilibrated enstatite chondrites. *Geochemistry* **72**, 101–115 (2012).
5. Marty, B. The origins and concentrations of water, carbon, nitrogen and noble gases on Earth. *Earth and Planetary Science Letters* **313–314**, 56–66 (2012).
6. Morbidelli, A. *et al.* Source regions and timescales for the delivery of water to the Earth. *Meteoritics & Planetary Science* **35**, 1309–1320 (2000).
7. Owen, T. & Bar-Nun, A. Comets, Impacts, and Atmospheres. *Icarus* **116**, 215–226 (1995).
8. Alexander, A. *et al.* The Provenances of Asteroids, and Their Contributions to the Volatile Inventories of the Terrestrial Planets. *Science* **337**, 721–723 (2012).
9. Piani, P. *et al.* Earth's water may have been inherited from material similar to enstatite chondrite meteorites. *Science* **369**, 1110–1113 (2020).

10. Gray, M. L., Weisberg, M. K., Alexander, C. M. O., Wang, J. & Ebel, D. S. H<sub>2</sub>O Abundances of an EH6 Chondrite and Potential Implications for Earth. in vol. 2695 6452 (2022).
11. Steller, T., Burkhardt, C., Yang, C. & Kleine, T. Nucleosynthetic zinc isotope anomalies reveal a dual origin of terrestrial volatiles. *Icarus* **386**, 115171 (2022).
12. Martins, R., Kuthning, S., Coles, B. J., Kreissig, K. & Rehkämper, M. Nucleosynthetic isotope anomalies of zinc in meteorites constrain the origin of Earth's volatiles. *Science* **379**, 369–372 (2023).
13. Savage, P. S., Moynier, F. & Boyet, M. Zinc isotope anomalies in primitive meteorites identify the outer solar system as an important source of Earth's volatile inventory. *Icarus* **386**, 115172 (2022).
14. Piani, L. *et al.* Structure, composition, and location of organic matter in the enstatite chondrite Sahara 97096 (EH3). *Meteoritics & planetary science* **47**, 8–29 (2012).
15. Thomassin, D. *et al.* The high-temperature origin of hydrogen in enstatite chondrite chondrules and implications for the origin of terrestrial water. *Earth and Planetary Science Letters* **616**, 118225 (2023).
16. Anzures, B., Parman, S., Milliken, R., Lanzirotti, A. & Newville, M. XANES Spectroscopy of Sulfides Stable under Reducing Conditions. *American Mineralogist* (2019) doi:10.2138/am-2020-7146.
17. Lerner, A. H. *et al.* Improving the reliability of Fe- and S-XANES measurements in silicate glasses: Correcting beam damage and identifying Fe-oxide nanolites in hydrous and anhydrous melt inclusions. *Chemical Geology* **586**, 120610 (2021).
18. Prange, A. *et al.* Investigation of S-H bonds in biologically important compounds by sulfur K-edge X-ray absorption spectroscopy. *The European Physical Journal D - Atomic, Molecular, Optical and Plasma Physics* **20**, 589–596 (2002).

19. Fleet, M. E. Xanes spectroscopy of sulfur in earth materials. *The Canadian Mineralogist* **43**, 1811–1838 (2005).
20. Klimm, K., Kohn, S. C. & Botcharnikov, R. E. The dissolution mechanism of sulphur in hydrous silicate melts. II: Solubility and speciation of sulphur in hydrous silicate melts as a function of fO<sub>2</sub>. *Chemical Geology* **322–323**, 250–267 (2012).
21. Métrich, N., Berry, A. J., O'Neill, H. St. C. & Susini, J. The oxidation state of sulfur in synthetic and natural glasses determined by X-ray absorption spectroscopy. *Geochimica et Cosmochimica Acta* **73**, 2382–2399 (2009).
22. Head, E., Lanzirotti, A., Newville, M. & Sutton, S. Vanadium, sulfur, and iron valences in melt inclusions as a window into magmatic processes: A case study at Nyamuragira volcano, Africa. *Geochimica et Cosmochimica Acta* **226**, 149–173 (2018).
23. Bodeur, S. & Esteve, J. M. Photoabsorption spectra of H<sub>2</sub>S, CH<sub>3</sub>SH and SO<sub>2</sub> near the sulfur K edge. *Chemical Physics* **100**, 415–427 (1985).
24. Wilke, M. *et al.* The origin of S<sup>4+</sup> detected in silicate glasses by XANES. *American Mineralogist* **93**, 235–240 (2008).
25. Lehner, S. W., McDonough, W. F. & Németh, P. EH<sub>3</sub> matrix mineralogy with major and trace element composition compared to chondrules. *Meteoritics & Planetary Science* **49**, 2219–2240 (2014).
26. Macke, R. J., Consolmagno, G. J., BRITT, D. T. & HUTSON, M. L. Enstatite chondrite density, magnetic susceptibility, and porosity. *Meteoritics & Planetary Science* **45**, 1513–1526 (2010).
27. Rubin, A. E., Griset, C. D., CHOI, B.-G. & WASSON, J. T. Clastic matrix in EH<sub>3</sub> chondrites. *Meteoritics & Planetary Science* **44**, 589–601 (2009).
28. Okada, A., Keil, K. & Taylor, G. J. Unusual weathering products of oldhamite parentage in the norton county enstatite achondrite. *Meteoritics* **16**, 141–152 (1981).

29. Bland, P. A., Zolensky, M. E., Benedix, G. K. & Sephton, M. A. Weathering of Chondritic Meteorites. in 853 (2006).
30. Avril, C. *et al.* Aqueous alteration and bioalteration of a synthetic enstatite chondrite. *Meteoritics and Planetary Science* **56**, 601–618 (2021).
31. Peterson, L. D. *et al.* The H content of aubrites: An evaluation of bulk versus in situ methods for quantifying water in meteorites. *Earth and Planetary Science Letters* **620**, 118341 (2023).
32. Schrader, D. L. *et al.* The Fe/S ratio of pyrrhotite group sulfides in chondrites: An indicator of oxidation and implications for return samples from asteroids Ryugu and Bennu. *Geochimica et Cosmochimica Acta* **303**, 66–91 (2021).
33. Piani, L., Marrocchi, Y., Libourel, G. & Tissandier, L. Magmatic sulfides in the porphyritic chondrules of EH enstatite chondrites. *Geochimica et Cosmochimica Acta* **195**, 84–99 (2016).
34. Harries, D. & Langenhorst, F. The nanoscale mineralogy of Fe,Ni sulfides in pristine and metamorphosed CM and CM/CI-like chondrites: Tapping a petrogenetic record. *Meteoritics & Planetary Science* **48**, 879–903 (2013).
35. Zolensky, M. E. & Thomas, K. L. Iron and iron-nickel sulfides in chondritic interplanetary dust particles. *Geochimica et Cosmochimica Acta* **59**, 4707–4712 (1995).
36. Kerridge, J. F. Formation of iron sulphide in solar nebula. *Nature* **259**, 189–190 (1976).
37. Gainsforth, Z. *et al.* Insights into solar nebula formation of pyrrhotite from nanoscale disequilibrium phases produced by H<sub>2</sub>S sulfidation of Fe metal. *American Mineralogist* **102**, 1881–1893 (2017).
38. Namur, O. *et al.* Melting processes and mantle sources of lavas on Mercury. *Earth and Planetary Science Letters* **439**, 117–128 (2016).
39. NASA. Antarctic Meteorite Petrographic Description. vol. 2023 (2022).

## Supporting Information Text

### Methods

#### Gaussian Peak Fitting

The energy and shape of a peak in an S-XANES spectrum is controlled by: the redox state of sulfur; the cation; the bond character; and the local bonding environment<sup>1</sup>. Unlike more oxidised sulfur compounds, sulfides (S<sup>2-</sup>) with differing cations display characteristic spectra with peaks at specific energies and with distinct shapes<sup>2</sup>. As such, species such as H-S produce a characteristic peak within the S-XANES spectrum. These absorption peak amplitudes are proportional to species abundance<sup>2</sup>, allowing for quantitative estimates of the concentrations of different sulfur species within complex geological samples, such as meteorites.

In order to extract peak amplitudes corresponding to iron sulfide and H-S in LAR 12252, we fitted 3 Gaussian curves simultaneously across the energy range 2468 – 2478 eV. The first 2 Gaussians of equal width fit to FeS at ~2471.4eV (depending on stoichiometry) and H-S at ~2473.2eV. A third curve of larger width was fit around 2478eV, corresponding to the second absorption peak of FeS and the step at the S K edge. Although a Gaussian only approximates the shape of this wider feature, we don't use it explicitly for any analysis, and the quality of fit in this part of the spectra is therefore less important than around the FeS and H-S peaks. The combined amplitudes of the peaks produced very small fitting errors against the measured spectrum. Gaussian curves fitted to FeS and H-S peaks were constrained by energy (eV) boundaries 2470.8 < FeS < 2472, 2472 < H-S < 2474, and maximum (1.5 eV) and minimum (0 eV) widths, to ensure that fitting was consistent and accurate between different spectra. Certain fits were manually rejected and excluded from calculations where it was obvious that the spectra contained high noise levels or spurious points. This was most common in spectra with very low sulfur counts (e.g., in the interiors of macroscale metal or enstatite grains), or in unique sulfide mineralogies such as niningerite.

Despite differences in monochromator calibration meaning peaks were not in the locations typically stated in the literature, it was possible to re-calibrate our values to align with literature values. The identity of the FeS peak was known based on optical observations of troilite. Both H-S and FeS are shifted by very similar energies, meaning we can confidently ascribe the peak we find at 2473.2eV to H-S, rather than native sulfur or pyrite, which are typically located at 2472 and 2471.6eV respectively (ref. 3).

Sulfur Species	Peak Location (eV) (This study)	Peak Location (eV) (Other studies)	Difference (eV)
FeS	2471.8	2470.7	1.1
H-S	2473.2	2472.3	0.9
S <sup>6+</sup>	2483.2	2482.1	1.1

**Table S1.** Locations of peaks in this study against other studies. Peak locations for FeS and S<sup>6+</sup> taken from ref. 3, H-S from ref. 4. H-S literature measurements are commonly performed on gaseous material, possibly accounting for small energy discrepancies.

#### H concentration calculation

In order to calculate the contribution of H-S to the total EH3 hydrogen budget, it was necessary to compare the amplitude of the H-S peak in fine matrix to a phase with known H concentrations, chondrule mesostasis, under the assumption that all mesostasis H is in the form H-S. The H concentration of mesostasis in EH3 chondrites has been measured<sup>5,6</sup> several times ( $n_1$ ) across a number of chondrules and meteorites using background-corrected nano-SIMS, with an average concentration of 706 ppm H, ( $\bar{C}_{H \text{ Mesostasis (SIMS)}}$ ).

$$\bar{C}_{H \text{ Mesostasis (SIMS)}} = \frac{\sum \text{SIMS Measurements}}{n_1}$$

We measured S-XANES spot spectra at 15 ( $n_2$ ) individual points within chondrule mesostasis (fig. S8). We recovered the amplitude of the H-S peak from each of these spectra using our multi-peak fitting method, and calculated the average amplitude,  $\overline{Amp}_{\text{Mesostasis}}$ .

$$\overline{Amp}_{Mesostasis} = \frac{\sum Mesostasis\ peak\ amplitudes}{n_2}$$

We then calculated the abundance of H-S at each point throughout our region of matrix, relative to mesostasis, by normalizing the H-S peak amplitude from each individual point to  $\overline{Amp}_{Mesostasis}$ . An average, representative hydrogen concentration for the mapped area, *H conc*, was then calculated by multiplying the relative peak amplitude by the average mesostasis hydrogen concentration, and dividing the sum by the number of points in the area ( $n_3$ ).

$$H\ conc = \frac{\sum \left( \frac{Point\ Peak\ Amp}{\overline{Amp}_{Mesostasis}} \times \overline{C}_{H\ Mesostasis\ (SIMS)} \right)}{n_3}$$

### Weathering

Enstatite chondrites are particularly susceptible to weathering on Earth. The detection of an S<sup>6+</sup> peak in our spectra demonstrates the presence of some terrestrial alteration products throughout our region of interest. As discussed in the main text, the total absence or small amplitude presence of H-S peaks in spectra collected from cracks argues the H-S peak is instead native to the enstatite chondrites. Nonetheless, we chose to exclude points in our analysis that contained evidence of more extensive terrestrial weathering. Based on the findings of ref. 7, FeS reacts on Earth to produce sulphates. As such, we chose to limit the spectra analyzed to those with a low S<sup>6+</sup>:FeS peak amplitude ratio, selected to be <0.5. This threshold ensured a significant number of data points were still analyzed while excluding regions of the meteorite that were exposed to more extensive terrestrial weathering products.

Notably, when points with higher ratios were included in our analysis, the average relative H-S amplitude decreased. This trend suggests that weathering reactions may actually have decreased the amount of hydrogen stored as H-S. This is consistent with our proposal that H-S is stored of grains of pyrrhotite, because weathering would act to remove the host phase of H-S through destruction of this mineral.

### Sources of error

Given the total bulk H content is calculated using H concentration in mesostasis ( $\overline{C}_{H\ Mesostasis\ (SIMS)}$ ) from refs. 5,6, possible errors in these literature data will carry through to the value calculated in this study.

An additional source of error in our calculations comes from difficulties in defining clastic matrix and fine matrix, which have varied definitions in the literature<sup>8-10</sup>. We minimised this error by targeting an area with few large clasts, and averaging matrix volumes from the literature<sup>8-10</sup>.

Additionally, there is potential for some error derived from the compositional difference of matrix and mesostasis when comparing peak amplitudes measured in the two phases. Based on our mesostasis S-XANES spectra that demonstrate sub-micron scale sulfides that exist in the mesostasis, as well as the FeS:H-S peak ratio being consistent between mesostasis and matrix, we propose that the carrier of H-S could be sulfide grains in both the mesostasis and fine matrix. As such, a correction between the two phases is not required.

There are inevitably sources of error in other aspects of the experiment, namely peak fitting, though our peak fitting produces only small residual errors (Fig. 1b), typically limited to around 1% of the peak absorption intensity. Given the size of these errors, we only present errors derived from SIMS measurements by ref. 5, as they are likely the dominant source, though acknowledge that other small errors are likely to be present in this total.

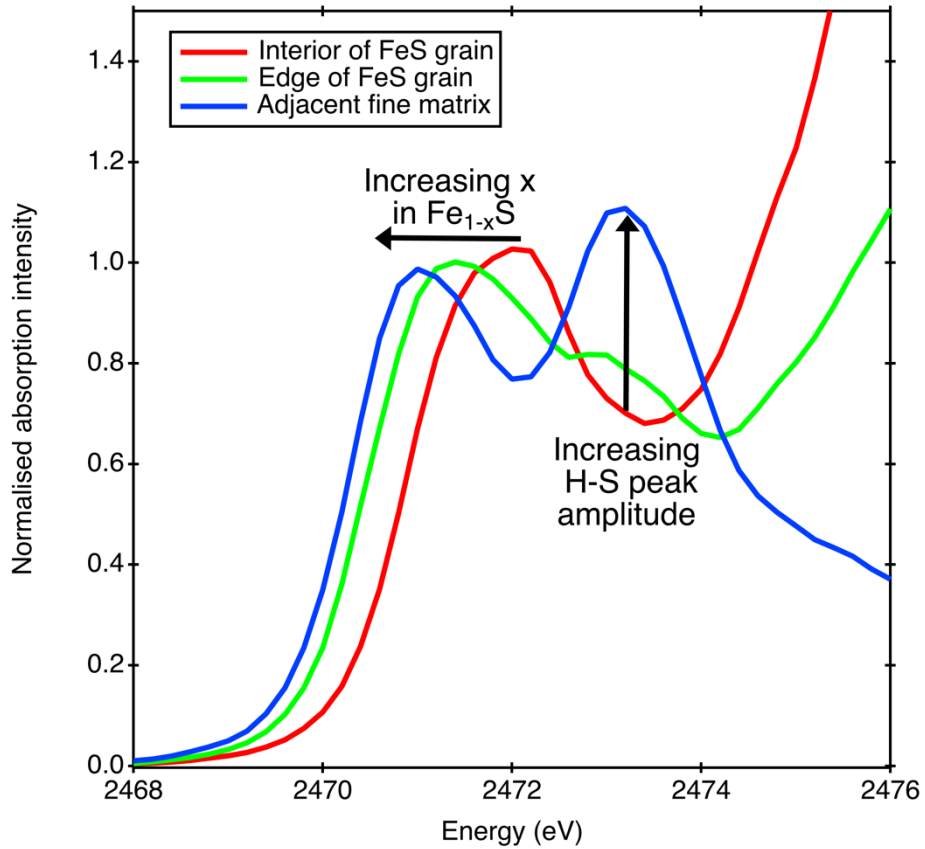


**Fig. S1.** XANES spectra with amplitude normalized at the FeS peak. The red spectra is taken from the interior of a grain of troilite (FeS). The green spectra is taken from the edge of that FeS grain. The blue spectrum is from the fine matrix just outside of this FeS grain. As the spectra move from the interior of a macroscale sulfide to the fine matrix, the position of the iron sulfide peak shift the lower energy and the relative amplitude of the H-S peak increases. The lateral shift in FeS peak position is indicative of the increase in  $x$  in  $\text{Fe}_{1-x}\text{S}$ , moving from troilite to pyrrhotite. Together, these trends argue that H is found in grains of pyrrhotite.

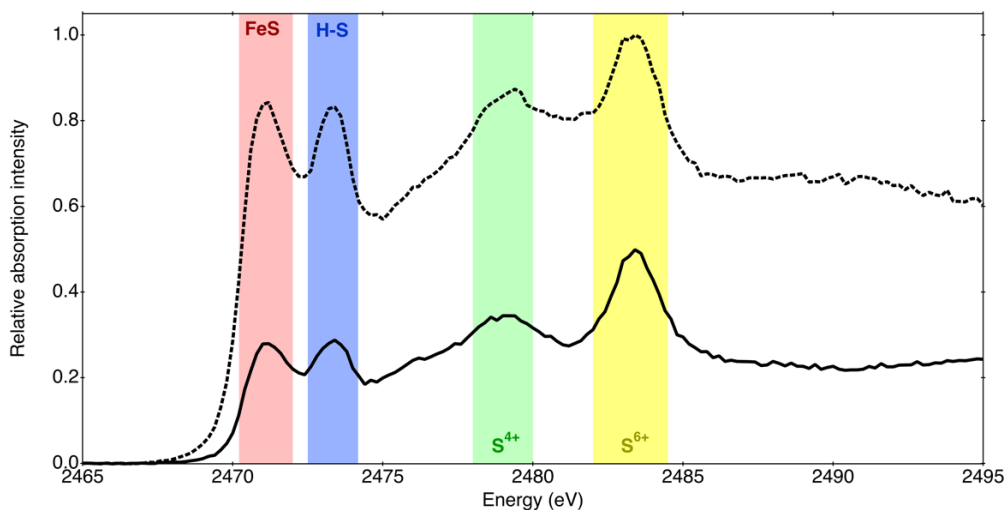


**Fig. S2.** Two spectra from matrix points in LAR 12252, marked by the solid and dashed lines, both normalized to maximum absorption intensity at  $\sim 2483\text{eV}$ . The ratio between FeS and H-S peak amplitude is similar in these spectra, and others throughout the matrix, demonstrating that H-S concentration is tied to the abundance of iron sulfides. Notably, the absolute amplitude of the peaks varies greatly throughout different areas of matrix in the meteorite, demonstrating the heterogeneity in H-S and iron sulfide abundance.

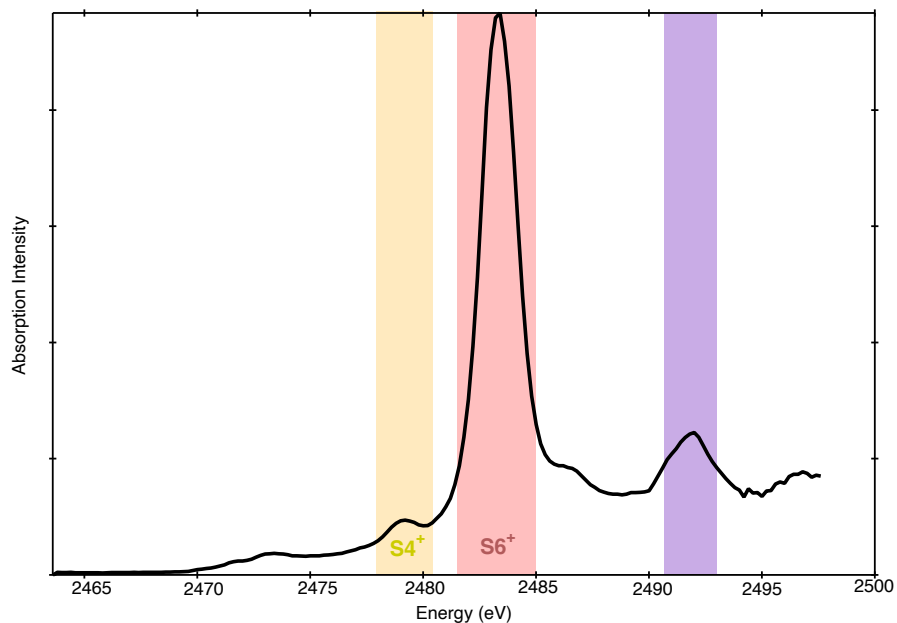


**Fig. S3.** XANES spot spectrum collected from a crack in LAR 12252. The high amplitude peak at ~2483eV corresponds to the presence of  $S^{6+}$ -bearing species, which is a terrestrial weathering product. The spectrum contains a small peak at 2473.2eV, though it is very small relative to the  $S^{6+}$  peak, suggesting that H-S is not a weathering product, but instead a small amount of native H-S that survived terrestrial weathering.

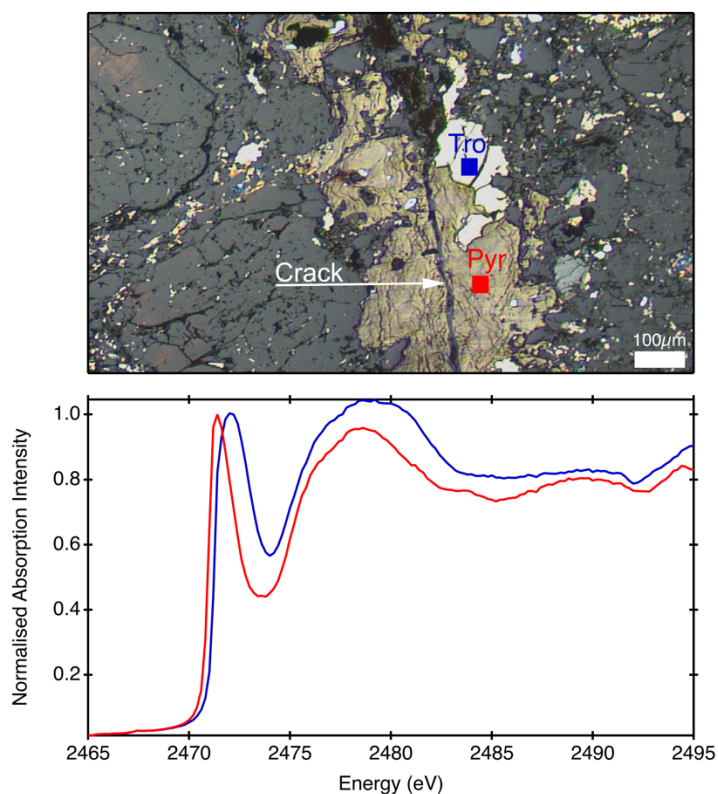


**Fig. S4.** XANES Spectra collected from two points within a terrestrially altered crack within the meteorite, with their amplitudes normalized at the initial FeS absorption peak at ~2471.4eV. The blue point represents the spot where the blue spectrum was collected and is a grain of stoichiometric FeS (troilite). The red square is the location where the



spectrum in red was collected, and is a grain of non-stoichiometric FeS, pyrrhotite. The pyrrhotite lithology here fills in a clear crack, suggesting that it is of terrestrial origin. Notably, this terrestrial pyrrhotite does not contain a peak at 2473.4eV, demonstrating it is devoid of H-S.

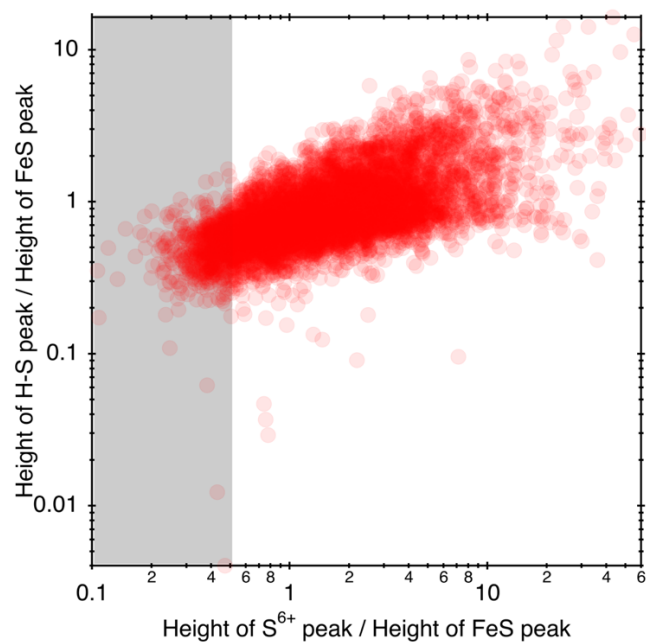


**Fig. S5.** Plot showing relative amplitude of H-S peak against relative amplitude of S<sup>6+</sup> peak, in spectra containing detectable H-S peaks. The positive trend of data points can be explained by the fact that FeS is the source of both native H-S, locked in the structure of non-stoichiometric pyrrhotite, and S<sup>6+</sup> produced in terrestrial weathering reactions of FeS. To avoid the influence of terrestrial weathering we limited analysis to points where S<sup>6+</sup>/FeS was below 0.5, as shown by the grey box.

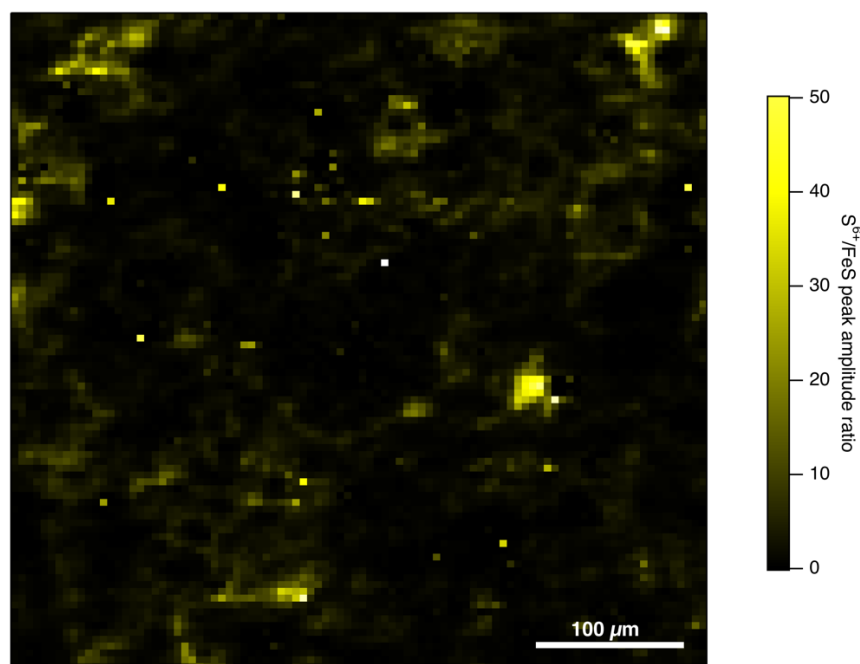


**Fig. S6.** Plot showing XANES map of S<sup>6+</sup>/FeS peak amplitude across the mapped area. S<sup>6+</sup> abundance is very heterogeneous, suggesting terrestrial weathering products are mostly in situ at the position of the previous sulfides. The corresponding optical image is shown in Fig 2a.

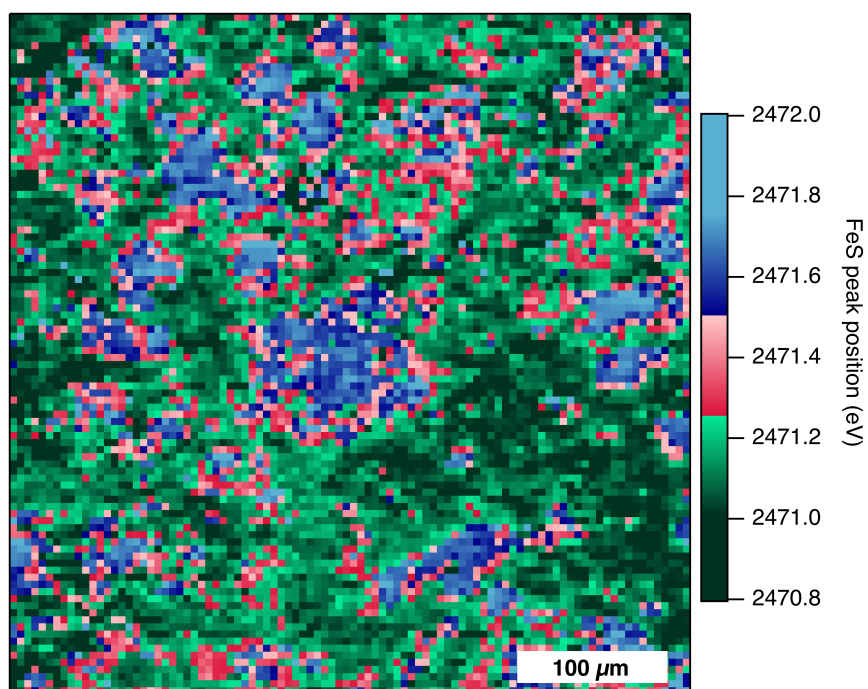


**Fig. S7.** XANES map showing the peak position of the iron sulfide peak. In the center of sulfide grains, the peak is located toward 2472.0eV, indicating the presence of stoichiometric FeS (troilite). At the rims of these grains, and into the matrix material surrounding them the peak position shifts to lower energy, indicating that iron sulfides are not stoichiometric (ref 11). The corresponding optical image is shown in Fig. 2a.

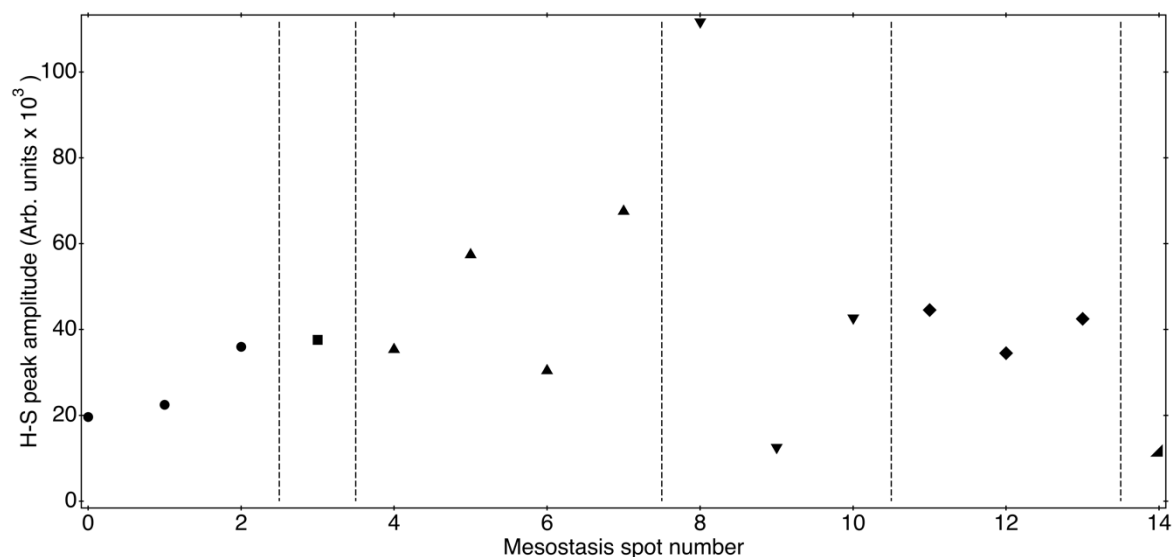


**Fig. S8.** H-S peak amplitudes taken from 15 spot spectra in chondrule mesostasis across 6 different chondrules. Chondrules are distinguished through different symbols, as well as dashed verticals separating them from each other. Measurements in each chondrule were taken from different patches of mesostasis within the chondrule.

#### Supporting References

1. Anzures, B., Parman, S., Milliken, R., Lanzirrotti, A. & Newville, M. XANES Spectroscopy of Sulfides Stable under Reducing Conditions. *American Mineralogist* (2019) doi:10.2138/am-2020-7146.
2. Fleet, M. E. Xanes spectroscopy of sulfur in earth materials. *The Canadian Mineralogist* **43**, 1811–1838 (2005).

3. Métrich, N., Berry, A. J., O'Neill, H. St. C. & Susini, J. The oxidation state of sulfur in synthetic and natural glasses determined by X-ray absorption spectroscopy. *Geochimica et Cosmochimica Acta* **73**, 2382–2399 (2009).
4. LaVilla, R. E. The sulfur K $\beta$  emission and K-absorption spectra from gaseous H<sub>2</sub>S. III. *The Journal of Chemical Physics* **62**, 2209–2212 (1975).
5. Piani, P. *et al.* Earth's water may have been inherited from material similar to enstatite chondrite meteorites. *Science* **369**, 1110–1113 (2020).
6. Thomassin, D. *et al.* The high-temperature origin of hydrogen in enstatite chondrite chondrules and implications for the origin of terrestrial water. *Earth and Planetary Science Letters* **616**, 118225 (2023).
7. Bland, P. A., Zolensky, M. E., Benedix, G. K. & Sephton, M. A. Weathering of Chondritic Meteorites. in 853 (2006).
8. Lehner, S. W., McDonough, W. F. & Németh, P. EH3 matrix mineralogy with major and trace element composition compared to chondrules. *Meteoritics & Planetary Science* **49**, 2219–2240 (2014).
9. Macke, R. J., Consolmagno, G. J., BRITT, D. T. & HUTSON, M. L. Enstatite chondrite density, magnetic susceptibility, and porosity. *Meteoritics & Planetary Science* **45**, 1513–1526 (2010).
10. Rubin, A. E., Griset, C. D., CHOI, B.-G. & WASSON, J. T. Clastic matrix in EH3 chondrites. *Meteoritics & Planetary Science* **44**, 589–601 (2009).
11. Head, E., Lanzirotti, A., Newville, M. & Sutton, S. Vanadium, sulfur, and iron valences in melt inclusions as a window into magmatic processes: A case study at Nyamuragira volcano, Africa. *Geochimica et Cosmochimica Acta* **226**, 149–173 (2018).